NEURAL REGENERATION RESEARCH
www.nrronline.org

Research Article

Müller cells are activated in response to retinal outer nuclear layer degeneration in rats subjected to simulated weightlessness conditions

Yuxue Mu[1, 2, #], Ning Zhang[3, #], Dongyu Wei[1, #], Guoqing Yang[1], Lilingxuan Yao[4], Xinyue Xu[1], Yang Li[5], Junhui Xue[1, 2, *], Zuoming Zhang[1, *], Tao Chen[1, 2, *]

https://doi.org/10.4103/NRR.NRR-D-23-01035
Date of submission: June 23, 2023
Date of decision: October 25, 2023
Date of acceptance: January 7, 2024
Date of web publication: March 1, 2024

From the Contents

Graphical Abstract

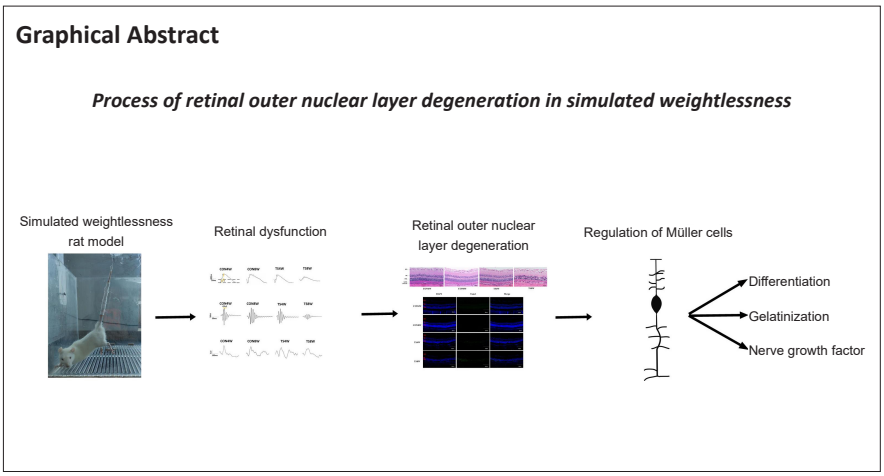

Abstract

A microgravity environment has been shown to cause ocular damage and affect visual acuity, but the underlying mechanisms remain unclear. Therefore, we established an animal model of weightlessness via tail suspension to examine the pathological changes and molecular mechanisms of retinal damage under microgravity. After 4 weeks of tail suspension, there were no notable alterations in retinal function and morphology, while after 8 weeks of tail suspension, significant reductions in retinal function were observed, and the outer nuclear layer was thinner, with abundant apoptotic cells. To investigate the mechanism underlying the degenerative changes that occurred in the outer nuclear layer of the retina, proteomics was used to analyze differentially expressed proteins in rat retinas after 8 weeks of tail suspension. The results showed that the expression levels of fibroblast growth factor 2 (also known as basic fibroblast growth factor) and glial fibrillary acidic protein, which are closely related to Müller cell activation, were significantly upregulated. In addition, Müller cell regeneration and Müller cell gliosis were observed after 4 and 8 weeks, respectively, of simulated weightlessness. These findings indicate that Müller cells play an important regulatory role in retinal outer nuclear layer degeneration during weightlessness.

Key Words: glial fibrous acidic protein; gliosis; Müller cells; nerve growth factor; neural differentiation; neurodegeneration; proteomic; retinal degeneration; retinal outer nuclear layer; simulated weightlessness

Introduction

Studies have shown that microgravity or simulated microgravity causes pathophysiological changes in the human body, which mainly manifest as muscle atrophy, bone loss (Ikeda et al., 2012; Blottner et al., 2023), cardiovascular dysfunction (Navasiolava et al., 2020), immune suppression (Fitzgerald et al., 2009), and changes in digestive system function (Yang et al., 2020). Research has shown that approximately 23% of astronauts who go on short-term missions and 53% of astronauts on long-term international space station missions experience functional changes in their vision (Yang et al., 2022). When astronauts enter microgravity, a series of ocular changes can occur, typically including unilateral thickening of the retinal nerve fiber layer, bilateral optic disc edema, globe flattening, formation of choroidal and retinal folds, the appearance of local retinal ischemia (cotton wool spots), and the development of hyperopic refractive error shifts (Lee et al., 2020; Wojcik et al., 2020; Ong et al.,

[1]Aerospace Clinical Medical Center, School of Aerospace Medicine, Air Force Medical University, Xi'an, Shaanxi Province, China; [2]Department of Aviation Medicine, Xijing Hospital, Air Force Medical University, Xi'an, Shaanxi Province, China; [3]Department of Emergency Medicine, Wuhan No.1 Hospital, Wuhan, Hubei Province, China; [4]Third Regiment, School of Basic Medicine, Air Force Medical University, Xi'an, Shaanxi Province, China; [5]Fourth Regiment, School of Basic Medicine, Air Force Medical University, Xi'an, Shaanxi Province, China
*Correspondence to: Tao Chen, PhD, ct1988@fmmu.edu.cn; Zuoming Zhang, PhD, zhangzm@fmmu.edu.cn; Junhui Xue, PhD, xuejunhui@fmmu.edu.cn.
https://orcid.org/0000-0003-4721-0163 (Tao Chen)
#These authors contributed equally to this work.

Funding: *This study was supported by the Army Laboratory Animal Foundation of China, No. SYDW[2020]22 (to TC); the Shaanxi Provincial Key R&D Plan General Project of China, No. 2022SF-236 (to YM); and the National Natural Science Foundation of China, No. 82202070 (to TC).*
How to cite this article: *Mu Y, Zhang N, Wei D, Yang G, Yao L, Xu X, Li Y, Xue J, Zhang Z, Chen T (2025) Müller cells are activated in response to retinal outer nuclear layer degeneration in rats subjected to simulated weightlessness conditions. Neural Regen Res 20(7):2116-2128.*

2022). These alterations are defined as spaceflight-associated neuro-ocular syndrome by the National Aeronautics and Space Administration, and may lead to long-term or permanent visual impairment in astronauts if timely intervention or treatment is not provided (Zhang and Hargens, 2018). In addition, this visual impairment affects the execution of flight tasks and threatens the personal safety of astronauts. The exact mechanism by which these eye changes occur is unclear; however, astronauts in microgravity may experience elevated intracranial pressure, nervous system changes, biochemical changes, and obstruction of the lymphatic and venous systems, which can lead to eye damage (Galdamez et al., 2020). Müller cells play an essential role in maintaining retinal structure and function through their extensive contacts with neurons, microvessels, and protrusions throughout the retina (Song et al., 2023). Müller cells are responsible for a diverse range of actions aimed at preserving retinal homeostasis and triggering defensive mechanisms in response to retinal injury (Coughlin et al., 2017; Reichenbach and Bringmann, 2020). A previous study showed that Müller cells serve as endogenous stem cells within the retinas of non-mammalian vertebrates following retinal damage, facilitating the regeneration of retinal neurons after injury (Reichenbach and Bringmann, 2020; Leinonen et al., 2023; Wang et al., 2023; Xu et al., 2023). Additionally, Müller cells in rodent retinas exhibit a gene expression profile that closely resembles that of retinal progenitor cells, and can undergo proliferation and dedifferentiation and promote glial proliferation in response to injury and retinal disease (Jian et al., 2015; Xiong et al., 2019; Niu et al., 2021). Each Müller cell is connected to one cone cell, approximately ten optic rods, and a variable number of intraretinal neurons, forming a columnar structure that serves as the fundamental and indispensable unit responsible for the transduction of visual information in the forward direction (Karlen et al., 2020). Furthermore, abnormal Müller cell activation leads to glial cell cycle progression, and the overactivation and cell cycle progression of Müller cells located within the subretinal region ultimately results in glial scarring with outer segmental fragments and increased photoreceptor cell apoptosis (Bejarano-Escobar et al., 2017). Therefore, Müller cell glial proliferation has emerged as a significant focal point in the fields of retinal disorder and visual regeneration research. The classic animal model used to simulate microgravity is tail suspension hind-limb unloading, which can be used to study diseases that may occur during space missions (Morey-Holton and Globus, 1998). Here, this model was used to observe Müller cell progression from neural regeneration to gliosis formation in microgravity and to clarify their role in retinal injury repair.

Methods

Animals

The 40 male specific-pathogen–free Sprague–Dawley rats, weighing 200 ± 20 g, aged 8 weeks, used in this study were obtained directly from the Laboratory Animal Center of Air Force Medical University, China (license No. SCXK 2019-001). All animal experiments were approved by the Animal Ethics Committee of the Air Force Medical University (approval No. IACUC-20220609) in June 2022. The animals were cared for in accordance with the Association for Research in Vision and Ophthalmology guidelines regarding the use of animals in scientific research (Association for Research in Vision and Ophthalmology, 2021). The rats were housed in a climate-controlled animal facility for 1 week with a 12/12-hour light/dark cycle, *ad libitum* access to both food and water, an ambient temperature of 23 ± 1°C, and a relative humidity level of approximately 50%. After 1 week, retinal function was evaluated by visual electrophysiology, and any rats that exhibited atypical retinal activity were excluded. The remaining rats were randomly divided into four groups (n = 6 rats/group): tail suspension for 4 weeks (TS4W), tail suspension for 8 weeks (TS8W), and one control group for each time point.

Construction of the simulated weightlessness model

To establish the model, which involves hind-limb unloading with the use of tail suspension (Morey-Holton and Globus, 2002), rats were suspended by their tails in an acrylic cage (Xi'an Shuguang Organic Glass Products Co., Ltd., Xi'an, China) measuring 26 cm × 26 cm × 30 cm, with their heads at a downward angle of –30°. First, each rat's tail was cleaned and air-dried. Then, a traction band was placed around the proximal section of the tail and secured to the tail by means of three circular pieces of adhesive tape. Next, the traction band was affixed to a stainless steel rod allowing unrestricted, 360° range of motion. The rats' visual parameters were assessed after 4 and 8 weeks of tail suspension. The control group (CON group) consisted of rats that were housed in a single cage under identical environmental conditions, but without hind-limb unloading or tail suspension.

Electroretinogram measurements

Prior to taking retinal function examination, the experimental animals were confined within a homemade dark adaptation box for more than 12 hours. Subsequently, a 1% sodium pentobarbital solution was administered via intraperitoneal injection at a dosage of 3 mL/kg (Sigma, St. Louis, MO, USA) to initiate anesthesia. Anesthetized rats were then treated with corneal surface anesthetic, followed by the application of 50 μL of an ocular eyedrop solution containing 10% librium (Jilin Shengda Animal Pharmaceutical Co., Ltd., Jilin, China), tropicamide (Shenyang Xingji Corporation, Shenyang, China), and orbucaine hydrochloride (Santen Pharmaceutical Co., Ltd., Osaka, Japan). The electroretinogram (ERG) measurements were subsequently carried out utilizing a computerized system (MonPack 3; Metrovision, Paris, France) equipped with full-field stimulation, following the guidelines outlined by the International Society for Clinical Electrophysiology of Vision (Bejarano-Escobar et al., 2017). The experiment involved the placement of three electrodes: recording electrode Ag-AgCl corneal ring electrode, reference electrode stainless-steel buccal needle electrode, and ground electrode stainless-steel tail needle electrode. Once these electrodes were positioned accordingly, the relevant ERG signals were recorded, after which the electrodes were extracted. Subsequently, gatifloxacin eye gel (Shenyang Xingji Corporation) was applied.

Pathological examination of retinal sections

Histological changes in the rat retina were examined by

hematoxylin-eosin (HE) staining of ocular sections. The rats were deeply anesthetized by intraperitoneal injection of pentobarbital (30 mg/kg; Sigma) and then sacrificed, after which their eyeballs were enucleated. The left eyeballs were immersed in a fixation solution consisting of acetic acid, formaldehyde solution, 75% alcohol, and normal saline in a ratio of 1:7:2:10. The fixed eyeballs were then dehydrated for 24 hours and subsequently embedded into wax blocks. Using a paraffin wax microtome, 4-μm sagittal sections were obtained along the vertical axis of the optic nerve papilla; a series of 10 consecutive sections was collected from each eye. After dehydration, the slices were stained with HE (Servicebio, Wuhan, China) and observed using a light microscope (Image-Pro® 10.0.1; Media Cybernetics, Inc., Rockville, MD, USA). All sections were centered on the optic disc and observed at intervals of 0.5 mm in both the nasal and temporal directions. Morphometric analysis involved quantification of the cells found within the inner nuclear layer and outer nuclear layer, as well as measurement of the inner segment and outer segment (IS/OS) layer thickness. Color micrographs were captured using a digital imaging system (Image-Pro® 10.0.1; Media Cybernetics, Inc.).

Terminal deoxynucleotidyl transferase deoxyuridine dUTP nick-end labeling staining of retinal sections

The retinal sections were subjected to dewaxing followed by two cycles of rinsing with xylene, following the detailed instructions provided in the terminal deoxynucleotidyl transferase dUTP nick-end labeling (TUNEL) assay kit (Servicebio). After the sections were subjected to dehydration using an alcohol gradient, the TUNEL reaction mixture was added. Subsequently, the sections were placed in a wet box for 2 hours. Following washing with phosphate-buffered saline (PBS), the tissues were restained with 4′,6-diamidino-2-phenylindole. Afterwards, fluorescein isothiocyanate was used to identify retinal cell apoptosis by laser confocal microscopy (CaseViewer, version 2.4, 3DHISTECH, Budapest, Hungary). Five randomly selected fields from each tissue slice were assessed.

Immunofluorescence staining of retinal sections

Paraffin-embedded sections were subjected to deparaffinization and dehydration, followed by endogenous peroxidase inhibition in a 3% H_2O_2 solution for 15 minutes. Subsequently, they were washed three times with 1× PBS of a specific concentration (pH 7.2) for 5 minutes each time. Then, antigen retrieval was performed by boiling at 100°C in citric acid buffer (pH 6.0) for 20 minutes. Afterwards, the sections were treated with a 10% goat serum solution containing 0.3% Triton for 1 hour to prevent non-specific labeling during staining. The tissue sections were then incubated overnight at 4°C with primary antibodies targeting sex determining region Y-box 2 (SOX2; mouse, Proteintech, Wuhan, China, Cat# 66411-1-Ig, RRID: AB_2881783), paired box gene 6 (PAX6; mouse; Proteintech; Cat# 12323-1-AP, RRID: AB_2159695), cellular retinaldehyde-binding protein (CRALBP; rabbit, Proteintech, Cat# 67529-1-Ig, RRID: AB_2882748), glial fibrous acidic protein (GFAP; rabbit, Proteintech, Cat# 16825-1-AP, RRID: AB_2109646), glutamine synthetase (GS; rabbit, Proteintech, Cat# 66323-2-Ig, RRID: AB_2881704), cone-rod homeobox (crx; rabbit, Proteintech, Cat# 12047-1-AP, RRID: AB_2292128), and rhodopsin (mouse, bs-19872R; Bioss, Beijing, China, Cat# 129-10588, RRID: AB_10565214) at 1:200 dilutions. Control slides were processed in the same way, but primary antibodies were not used. Afterward, the slides were rinsed three times in PBS, and the sections were then incubated with Cy3 fluorescence-labeled goat anti-mouse IgG secondary (1:10,000, Proteintech, Cat# SA00013-4, RRID: AB_2810984) and Alexa Fluor™ 488 fluorescence-labeled goat anti-rabbit IgG secondary antibodies (1:10,000, Proteintech, Cat# SA00013-2, RRID: AB_2797132) at 37°C for 2 hours. The nuclei were stained by immersing the sections in a solution containing 100 ng/mL of 4′,6-diamidino-2-phenylindole, followed by three successive rinses with PBS. Immunofluorescence images were captured using a fluorescence microscope (BX53; Olympus, Tokyo, Japan). The central area of each sagittal plane was identified within the retina, and retinal sections located within 2500 μm of the optic nerve were analyzed.

The quantitative proteomics assay utilizing tandem mass tag

Protein extraction

The experimental animals were anesthetized and sacrificed (n = 3) after 8 weeks of tail suspension. The eyeballs were collected, and the retinas were harvested immediately and transferred to a mortar that had been pre-cooled using liquid nitrogen. The samples were ground in liquid nitrogen to produce cellular powder, which was then transferred to a 5-mL centrifuge tube and treated with four volumes of buffer containing 8 mol/L urea and 1% protease inhibitor cocktail. The mixture was subjected to three cycles of sonication on ice using an intensive ultrasonic processor (Scientz; Ningbo, China). Cellular debris was eliminated by subjecting the homogenate to centrifugation at 12,000 × g for 10 minutes at 4°C. Subsequently, the supernatant of the sample was collected, and the protein concentration was determined using a bicinchoninic acid assay (BCA) kit (Beyotime Biotechnology, Shanghai, China) according to the manufacturer's instructions.

Trypsin digestion

Equal amounts of protein from each sample were subjected to digestion, as follows. A volume containing the appropriate amount of protein was adjusted with lysis solution so that all sample volumes were equal. The protein solution was then mixed with 20% trichloroacetic acid and vortexed thoroughly to combine. The samples were then allowed to precipitate for 2 hours at 4°C, after which they were centrifuged at 4500 × g for 5 minutes. Next, the supernatant was removed, and the precipitate was washed two or three times with pre-cooled acetone and allowed to dry. Triethylammonium bicarbonate buffer (TEAB) was added, resulting in a final protein concentration of 200 mM. The precipitate was then sonicated to disrupt the structure of the proteins, followed by the addition of trypsin at a ratio of 1:50 (protease:protein, m/m). The resulting mixture was left to digest overnight. Dithiothreitol was added the solution, to a final concentration of 5 mM, and the reduction process was allowed to proceed for 30 minutes at 56°C. Subsequently, iodoacetamide was

added to a final concentration of 11 mM, and the mixture was incubated for 15 minutes at ambient temperature in the dark.

Tandem mass tag/isobaric tags for relative and absolute quantitation (iTRAQ) labeling

Following trypsin digestion, the peptides were desalted utilizing a Strata X C18 solid-phase extraction column (Phenomenex; Green Baicao Scientific Instrument Co., Ltd., Guangzhou, China) and vacuum-dried. The peptides were then reconstituted in a solution of 0.5 M TEAB and subsequently processed using a tandem mass tag (TMT) kit (Thermo Fisher Scientific, Waltham, MA, USA) according to the manufacturer's instructions. Briefly, one unit of TMT reagent was thawed and then regenerated in acetonitrile. Subsequently, the peptide mixtures were incubated for 2 hours at an ambient temperature. Afterwards, the mixtures were combined, desalted, and vacuum-centrifuged to dry.

High-performance liquid chromatography fractionation

The sample was fractionated by high-pH reverse-phase high-performance liquid chromatography with an Agilent 300 Extend C18 column (5-μm particles, 4.6 mm ID, 250 mm length, PN770450902). Briefly, peptides were separated with a gradient of 8% to 32% acetonitrile in 10 mM ammonium bicarbonate pH 9 over 60 minutes into 60 fractions. Afterwards, the peptides were combined into 14 fractions and vacuum-centrifuged to dry.

Liquid chromatography-mass spectrometry/mass spectrometry assay

The tryptic peptides were dissolved in 0.1% formic acid (solvent A). Subsequently, they were introduced to an analytical column with reverse-phase features that was developed in-house (15 cm in length, 75 μm in diameter). The gradient involved a gradual changed from 6% to 23% of solvent B (0.1% formic acid in 98% acetonitrile) over 26 minutes. Subsequently, the concentration of solvent B increased from 23% to 35% over 8 minutes. Following this, there was a rapid increase to 80% within 3 minutes, which was maintained for the final 3 minutes of the process. An EASY-nLC 1000 UPLC machine was used with a consistent flow rate of 400 nanoliters per minute. The peptides were examined using a NSI source, followed by tandem mass spectrometry (MS/MS) analysis using a Q ExactiveTM Plus instrument (Thermo Fisher Scientific), which was coupled in real time to the UPLC system. The voltage employed for electrospray was 2.0 kV. The m/z scan range utilized for comprehensive scanning was between 350 and 1800. Intact peptides were subsequently identified in the Orbitrap mass spectrometer, operating at a resolution of 70,000. Subsequently, the peptides were selected for MS/MS at a normalized collision energy of 28, and the resulting fragments were observed in the Orbitrap mass spectrometer with a resolution of 17,500. The data-dependent procedure involved a sequential pattern of 1 MS scan followed by 20 MS/MS scans with a dynamic exclusion period of 15.0 seconds. Automatic gain control was configured to a value of 5E4, and the initial mass value was 100 m/z.

Database search

The MS/MS data acquired were analyzed using the Maxquant search engine (version 1.5.2.8; Matrix Science, Boston, MA, USA). Proteins whose expression exhibited a fold change of more than 1.3 or less than 1/1.3, as well as a *P*-value < 0.05 between two groups, were defined as differentially expressed proteins (DEPs). The tandem mass spectra were compared with a combined database including the human UniProt database (http://www.Uiport.org/) and the reverse decoy database. Trypsin/P was specified as the cleavage enzyme, allowing up to two missing cleavage events. During the first search, the mass tolerance for precursor ions was set at 20 ppm, while in the subsequent primary search it was decreased to 5 ppm. Furthermore, a mass tolerance of 0.02 Da was established for fragment ions. Cysteine carbamidomethylation was specified, as well as methionine acetylation and oxidation. The false discovery rate was set to below 1%, and at least 40 peptides needed to be counted to indicate a DEP.

Bioinformatics analysis

Gene Ontology (GO; http://www.geneontology.org) analysis was used for gene annotation. The Kyoto Encyclopedia of Genes and Genomes (KEGG; http://www.genome.jp/kegg/) and the Cluster of Orthologous Groups of proteins (COG) database (http://www.ncbi.nlm.nih.gov/COG/) were used along with the clusterProfiler package of R to identify DEP functions. The cut-off value for the GO enrichment analysis was set at $P < 0.05$. Significant KEGG pathways were defined using a threshold of $P < 0.05$. The Pearson correlation coefficient heat map was created using the R software package coreplot.

Western blot assay

Proteins were isolated from rat retinas and choroids, and protein concentrations were determined using a BCA kit according to the manufacturer's instructions (Beyotime Biotechnology). Briefly, 50 μL of 5× loading buffer was added to each protein sample, which were then boiled at 100°C for 15 minutes to denature the proteins. Afterwards, the denatured proteins were subjected to sodium dodecyl sulfate polyacrylamide gel electrophoresis (SDS-PAGE). Subsequently, the samples were transferred onto a polyvinylidene fluoride membrane for 90 minutes. The membrane was then stained at 4°C overnight with primary antibodies against the following proteins: hypoxia inducible factor-1α (HIF-1α; rabbit, Proteintech, Cat# 20960-1-AP, RRID: AB_10732601), Bcl-2 (rabbit, Proteintech, Cat# 26593-1-AP, RRID: AB_2818996), Bax (rabbit, Proteintech, Cat# 50599-2-Ig, RRID: AB_2061561), and caspase-3 (rabbit, Proteintech, Cat# 25546-1-AP, RRID: AB_2619655), diluted 1:1000; and glial fibrous acidic protein (GFAP; rabbit, Proteintech, Cat# 16825-1-AP, RRID: AB_2109646), GS (rabbit, Proteintech, Cat# 11037-2-AP, RRID: AB_2110650), L-glutamate/L-aspartate transporter (GLAST; rabbit, Cell Signaling Technology, Danvers, MA, USA, Cat# DZ003, RRID: AB_2335765), bFGF (rabbit, Bioss, Beijing, China, Cat# bs-0217R-FITC, RRID: AB_11054340), microtubule-associated protein 1 (MAP-1; rabbit, Abcam, Cambridge, UK, Cat# ab4132, RRID: AB_613591), glial cell-derived neurotrophic factor (GDNF; rabbit, ABclonal, Beijing, China, Cat# A14639, RRID: AB_2761514), and glyceraldehyde-3-photosphate dehydrogenase (GAPDH; mouse, Proteintech,

Cat# 66009-1-Ig, RRID: AB_2687938), diluted 1:2000. Next, the membrane was washed three times in Tween-PBS solution for 10 minutes each. The samples were then incubated with anti-rabbit (Cell Signaling Technology, Cat# 7074, RRID: AB_2099233) and anti-mouse (Cell Signaling Technology, Cat# 7076, RRID: AB_330924) secondary antibodies (both diluted 1:10,000) with shaking at ambient temperature for 1–2 hours. Subsequently, the membranes were washed three times with Tween-PBS for 10 minutes each time, followed by signal development, washing, and imaging. Quantity One software (Millipore, version 5.2.1, National Institutes of Health, Bethesda, MD, USA) was used to determine the average optical density value of all bands. Expression levels were normalized to GAPDH.

Statistical analysis

No statistical methods were used to predetermine sample sizes; however, our sample sizes were similar to those reported in a previous publication (Qu et al., 2018). No animals or data points were excluded from the analysis. In addition, the analysis was conducted by investigators who were blinded to the group assignments. Data are presented as the mean ± standard deviation. Significant differences between two groups were determined by independent samples *t*-test using GraphPad Prism software (v8.0.1, GraphPad Software, Inc., San Diego, CA, USA, www.graphpad.com). $P < 0.05$ was established as the threshold for statistical significance.

Results

Simulated weightlessness impairs retinal function

To determine whether simulated weightlessness can cause retinal damage, we evaluated retinal function by electroretinogram. The amplitude of dark-adapted 3.0 ERG signals reflects rod and cone function, whereas the amplitude of dark 3.0 oscillatory potential (OPs) ERG signals reflects retinal vascular function (Szabó-Salfay et al., 2001). In addition, the latency and amplitude of the visually evoked potential P1 wave reflects visual pathway function (Kondo et al., 2023). Compared with the CON group, the amplitude of the dark adaptation 3.0 response and OPs2 wave (dark adaptation 3.0 OPs response) was significantly reduced in the tail suspension group after 8 weeks ($P < 0.01$; **Figure 1A–E**). Moreover, HIF-1α expression was significantly increased in the retinal tissue of rats subjected to tail suspension compared with the CON group ($P < 0.01$; **Figure 1F** and **G**), suggesting that simulated weightlessness can lead to impaired ocular microcirculation and affect retinal function. Next, visual pathway function was detected by flash visual evoked potentials (Visual Physiology Group of Ophthalmology Branch of Chinese Medical Association and Visual Physiology Group of Chinese Ophthalmologist Association, 2023), and showed a significantly delayed peak time and reduced amplitude after 8 weeks of tail suspension compared with the CON group ($P < 0.01$; **Figure 1H–J**).

Simulated weightlessness alters retinal morphology

To determine whether simulated weightlessness can cause retinal damage, HE and TUNEL staining were performed to assess alterations in retinal structure and detect apoptosis, respectively. HE staining showed that, compared with the CON group, the IS/OS thickness (indicating optic cone and rod cell numbers) and the outer nuclear layer thickness were lower in the TS8W group ($P < 0.05$; **Figure 2A–C**). Furthermore, TUNEL staining showed a significant number of apoptotic cells in the outer nuclear layer after 8 weeks of tail suspension ($P < 0.01$; **Figure 2D** and **E**). Consistent with these findings, higher expression levels of the proapoptotic molecules Bax and Caspase 3 were detected in the TS8W group than in the CON group (**Figure 2F–I**). This suggests that tail suspension simulation of weightlessness can lead to degenerative changes in apoptosis of the outer nuclear layer cells of the rat retina.

Proteomic analysis of rat retinal tissue under weightless conditions

Sample protein information

Global changes in protein expression induced by weightlessness were characterized by employing a quantitative TMT proteomics strategy. A total of 7122 proteins were identified, and the expression of 6212 of these proteins was quantified (**Figure 3A–C**). A total of 212 DEPs were selected that exhibited a fold change in expression of > 1.3 and < 1/1.3 and a *P*-value of ≤ 0.05 (**Additional Table 1**), with 129 found to be up-regulated, while 83 were observed to be down-regulated (**Figure 3B** and **C**). Among these DEPs were bFGF and GFAP, which are closely related to Müller cell activation, and MAP-1, which is closely related to retinal neuronal repair (Kang et al., 2014). To ensure the reliability of the proteomic results, the control group and the TS8W group samples were tested for repeatability. The variation was graphed in relation to the proportion of the proteins that were identified, demonstrating the strong reliability of the proteomics data (**Additional Figure 1**).

Functional enrichment analysis of differentially expressed proteins based on Gene Ontology annotations

The DEPs were functionally annotated using GO analysis (**Figure 3D**) and assigned to one of three classes: biological process (BP), cellular component (CC), or molecular function (MF). The proteins within the BP category were found to be associated with various biological processes, including visual perception, sensory perception of light stimulus, detection of visible light, camera-type eye development, detection of visible light, eye morphogenesis, sensory perception of chemical stimulus, response to light intensity, photoreceptor cell differentiation, photoreceptor cell development, eye photoreceptor cell development, cellular response to light stimulus, and other related processes. The proteins within the CC category were predominantly predicted to be localized within cellular components, including the photoreceptor outer segment, ciliary membrane, photoreceptor disc membrane, photoreceptor cell cilium, extracellular matrix, and photoreceptor inner segment. The proteins within the MF category were found to be associated with molecular functions, including the structural component of the eye lens, structural molecule activity, extracellular matrix structural component, G-protein coupled photoreceptor activity, photoreceptor activity, guanylate cyclase regulator activity, and guanylate cyclase activator activity.

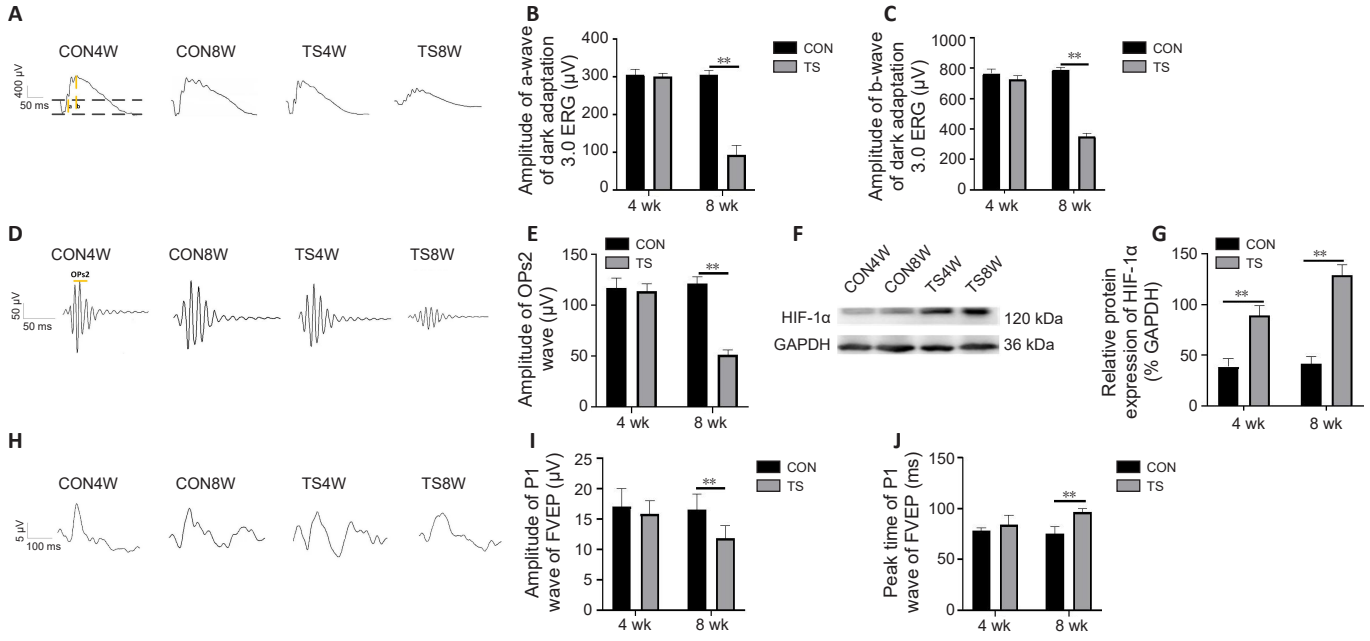

Figure 1 | **Effect of simulated weightlessness on retinal function and HIF-1α expression in the retina.**
(A) Representative images of a- and b-waves in the dark-adaptation 3.0 response. (B) Amplitude of the a-wave. The amplitude of the a-wave in the TS group was lower than that in the CON group. (C) Amplitudes of the b-waves. The amplitude of the b-wave in the TS group was lower than that in the CON group. (D) OPs2 wave (dark-adaptation 3.0 oscillatory potential response). (E) The amplitude of OPs2 wave. The amplitude of the OPs2 wave in the TS group were lower than that in the CON group. (F, G) Quantification of HIF-1α expression. HIF-1α expression in the TS group was lower than that in the CON group. (H) The amplitude of the FVEP wave. (I) The amplitude of the P1 wave of FVEP. The amplitude of the P1 wave of FVEP in the TS group was lower than that in the CON group. (J) The peak time of the P1 wave of FVEP. The peak time of the P1 wave of VEP in the TS group was lower than that in the CON group. Data are expressed as mean ± SD (n = 6 rats per group). $^{**}P < 0.01$ (independent samples t-test). CON: Control; FVEP: flash visual evoked potential; HIF-1α: hypoxia inducible factor-1α; TS4W: tail suspension for 4 weeks; TS8W: tail suspension for 8 weeks.

Classification of the Clusters of Orthologous Groups of proteins functions of the differentially expressed proteins

To provide a more comprehensive characterization of the DEPs, we also conducted Clusters of Orthologous Groups of proteins functional classification (**Figure 3E**). The DEPs were categorized into 18 distinct classes: 19 proteins were correlated with translation, ribosomal structure, and biogenesis; 15 proteins were involved in chromatin structure and dynamics; 10 proteins exhibited an association between signal transduction mechanisms and transcription; 7 proteins were associated with the cytoskeleton; 6 proteins were linked to protein turnover, posttranslational modification, and chaperones; 4 proteins exhibited an association with energy production and conversion, as well as the formation of extracellular structures; 3 proteins were linked to amino acid transport and metabolism, as well as mechanisms of defense; and 6 proteins exhibited a correlation with RNA processing and modification, nucleotide transport and metabolism, carbohydrate transport and metabolism, replication, recombination, and repair, secondary metabolite biosynthesis, transport and catabolism, intracellular trafficking, secretion, or vesicular transport. Notably, another six DEPs had no known function; hence, additional investigation is necessary to explore the role of these proteins.

Kyoto Encyclopedia of Genes and Genomes pathway analysis of the differentially expressed proteins

KEGG pathway analyses were performed to determine the fundamental signaling pathways involving the identified DEPs (**Figure 3F**). Our data suggest that the DEPs mainly participate in phototransduction, the phosphatidylinositol 3 kinase/protein kinase B (PI3K-AKT) signaling pathway, the relaxin signaling pathway, protein digestion and absorption, extracellular matrix (ECM)-receptor interactions, and glutamatergic synapses, all of which are closely related to retinal damage.

Simulated weightlessness stimulates Müller cell retrodifferentiation

To determine whether simulated weightlessness stimulates retrodifferentiation of Müller cells, the retinas were double stained for CRALBP (a marker of Müller glial cells (Jurkute and Robson, 2021)) and SOX2 or PAX6 (stem/progenitor cell markers (Lin et al., 2009)). As shown in **Figure 4A–D**, following 4 weeks of tail suspension, the rats exhibited massive activation of retinal Müller cells and a statistical increase in SOX2 and PAX6 expression compared with the CON group ($P <$ 0.01; **Figure 4B** and **D**). Following 8 weeks of tail suspension, a notable reduction was observed in the expression levels of SOX2 and PAX6, with SOX2 expression more greatly reduced ($P < 0.05$; **Figure 4B**). This suggests that tail suspension in rats effectively simulates weightlessness and stimulates retrodifferentiation of retinal Müller cells, which exhibit progenitor cell properties for a short period of time.

Simulated weightlessness stimulates Müller cell neurodifferentiation

To determine whether simulated weightlessness stimulates Müller cell neurodifferentiation, we performed

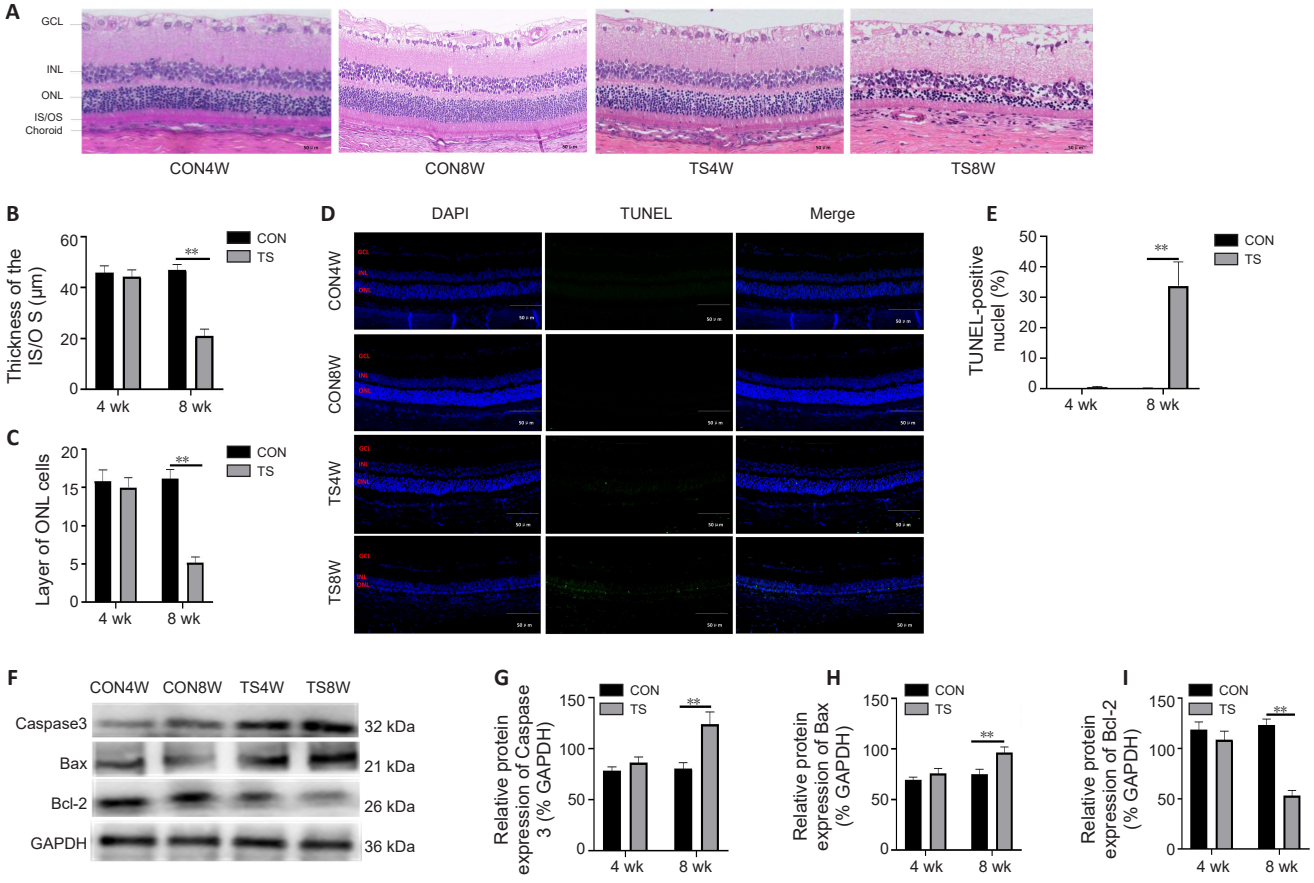

Figure 2 | **Effect of simulated weightlessness on retinal morphology in rats.**
(A) A typical HE staining image. (B) Quantification of IS/OS layer thickness. The IS/OS layer was thinner in the TS group than in the CON group. (C) ONL cell layer. The ONL cell layer in the TS group was thinner than that in the CON group. (D) Representative TUNEL staining images. The nuclei are shown in blue, while the apoptotic cells emitted green fluorescence. Scale bars: 50 μm. (E) Apoptosis rates in the outer retinal nuclear layer in each group of rats. The apoptosis rate was higher in the TS group than in the CON group. (F) Western blot images of Caspase 3, Bax, and Bcl-2. (G–I) Quantification of the relative expression levels of Caspase 3, Bax, and Bcl-2. Caspase 3 and Bax were expressed at higher levels in the TS group than in the CON group, and Bcl-2 expression was lower in the TS group than in the CON group. Data are expressed as mean ± SD (n = 4–6 per group). $^{**}P < 0.01$ (independent samples t-test). CON: Control; DAPI: 4′,6-diamidino-2-phenylindole; GAPDH: glyceraldehyde-3-photosphate dehydrogenase; GCL: ganglion cell layer; HE: hematoxylin-eosin; INL: inner nuclear layer; IS/OS: inner and outer segment layer; ONL: outer nuclear layer; RPE: retinal pigment epithelial; TS: tail suspension; TUNEL: terminal deoxynucleotidyl transferase deoxyuridine dUTP nick-end labeling.

immunofluorescence staining for crx and rhodopsin. Based on the results of proteomic analysis, we found that the expression of rhodopsin in the retina tissue of TS8W group rats decreased (**Additional Table 1**). Next, retinas were double stained for CRALBP and the photoprecursor/mature photoreceptor cell markers crx and rhodopsin. As shown in **Figure 5**, crx and rhodopsin expression levels were higher in the retinal tissues of rats in the TS4W group compared with the CON group ($P < 0.01$). This suggests that tail suspension simulates the early stage of weightlessness and promotes Müller cell neurodifferentiation.

The effect of simulated weightlessness on Müller cell gelatinization

To determine the effect of simulated weightlessness on gelatinization in retinal tissues, we detected the glial-associated marker GFAP and the glutamate (GLU) metabolism–related markers GS and GLAST in retinal tissues from rats in each group (**Figure 6**). Increased GFAP expression and decreased GS and GLAST expression were observed after 4 weeks of tail suspension compared with the CON group, although these differences were not statistically significant. GFAP expression was further increased ($P < 0.01$), and GS expression was further decreased ($P < 0.01$), in the retinal tissues of rats after 8 weeks of tail suspension compared with the CON group. GLAST is involved in the GLU cycle (Wunderlich et al., 2010), and significantly decreased GLAST expression was observed at 8 weeks of tail suspension ($P < 0.01$). Müller cells undergo a glial cell fate in the late stage of microgravity injury, which can affect GLU translocation and metabolism.

Glial cell-derived neurotrophic factor, basic fibroblast growth factor, and microtubule-associated protein 1 expression in the rat retina under simulated weightlessness conditions

Based on the results of proteomic analysis, GDNF, bFGF, and MAP-1 were selected as protein markers of retinal injury to investigate retinal impairment during simulated weightlessness. Compared with the CON group, GDNF, bFGF, and MAP-1 expression levels were higher in the retinas of rats in the TS4W and TS8W groups (all $P < 0.01$; **Figure 7**). This suggests that tail suspension effectively mimicked weightlessness, resulting in retinal damage and the subsequent upregulation of neurotrophic factors.

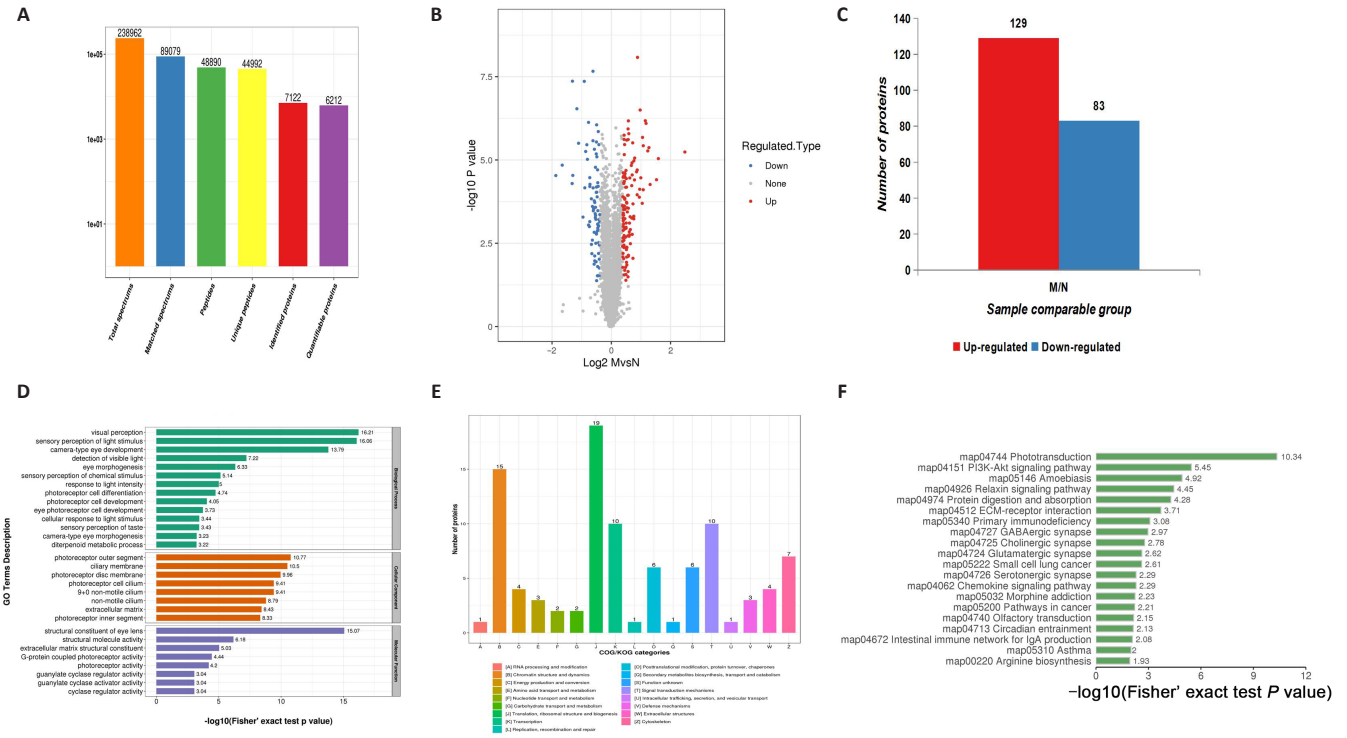

Figure 3 | **Proteomic analysis of the rat retina under simulated weightlessness conditions.**
(A) Fundamental mass spectrometry data statistics. (B) Volcano plot of DEPs in rat retinas in the TS group compared with the CON group. The horizontal axis represents the relative percentage of protein expression following Log2 logarithmic conversion, and the vertical axis indicates the level of statistical significance as determined by the *P*-value following-Log10 logarithmic conversion. Blue and red dots represent differential overexpression and underexpression of DEPs, respectively. (C) DEP distribution histogram. (D) Enriched DEPs in BPs. (E) Enriched DEPs in COG functional categories. Capital letters on the horizontal axis indicate the COG category plotted on the right side of the histogram, and the vertical axis shows the number of proteins in each category. (F) KEGG pathways. BP: Biological process; COG: Clusters of Orthologous Groups of protein; DEP: differentially expressed protein; KEGG: Kyoto Encyclopedia of Genes and Genomes; TS: tail suspension.

Discussion

The present study demonstrated that tail suspension for 8 weeks effectively simulated weightlessness, resulting in thinning of the outer retinal nucleus layer and degenerative changes. However, no changes in outer retinal nucleus layer thickness were observed following 4 weeks of tail suspension. To clarify the mechanism underlying the degenerative changes within the retina's outer nuclear layer under simulated weightlessness conditions, a proteomics approach was used to elucidate the pathological characteristics of the degenerative changes.

Microgravity can promote redistribution of body fluids and increase blood volume in the head and chest (Bringmann et al., 2009). These changes result in arterial constriction and venous stasis of ocular blood flow (Lee et al., 2020; Ercan, 2021). Furthermore, relatively short time periods spent in microgravity may lead to the development of retinal ischemia (Taibbi et al., 2013). The OPs wave, which is a constituent of the ERG test, is widely recognized as a valuable parameter for assessing retinal vascular diseases, specifically retinal ischemia resulting from compromised circulation (Wachtmeister, 1998; Dai et al., 2020). We observed diminished retinal vascular microcirculation and elevated HIF-1α expression in rats after simulated weightlessness via tail suspension. Similar fluctuations in OPs amplitude have been observed in other animal models of head-down simulated weightlessness and in humans (Zhao et al., 2016; He et al., 2021). Since retinal photoreceptors are more sensitive to retinal ischemia than other retinal cells, the negative ERG wave (dark-adaptation 3.0 response), namely the a-wave, appeared to be significantly suppressed following tail suspension. The findings presented herein elucidate the light absorption capacity of photoreceptors. Moreover, significant changes were observed in IS/OS thickness and the outer nuclear layer of the retina (photoreceptor cell layer), with the presence of apoptotic cells within the outer nuclear layer, indicating degeneration.

bFGF, MAP-1, and GFAP, which are closely related to Müller cell activation, were identified as markers of degeneration of the outer nuclear layer of the retina, confirming that Müller cells mediate retinal damage in microgravity. Ischemia/hypoxia or increased intraocular pressure can lead to Müller cell activation (Kergoat and Durand, 1996; Reichenbach et al., 2007; Dou et al., 2024). In higher vertebrates, retinal injury may trigger Müller cells to adopt progenitor cell properties and form new neurons (Kalesnykas et al., 2008). After 4 weeks of simulated weightlessness, Müller cells showed reverse differentiation and expression of stem/progenitor cell parameters, such as SOX2 and PAX6. Müller cells can reverse differentiate into retinal progenitor cells that transdifferentiate to express photoreceptor markers (crx and rhodopsin), which help repair the damage caused by retinal injury. However, the regenerative capacity of Müller cells is limited, and retrodifferentiation was almost completely lost

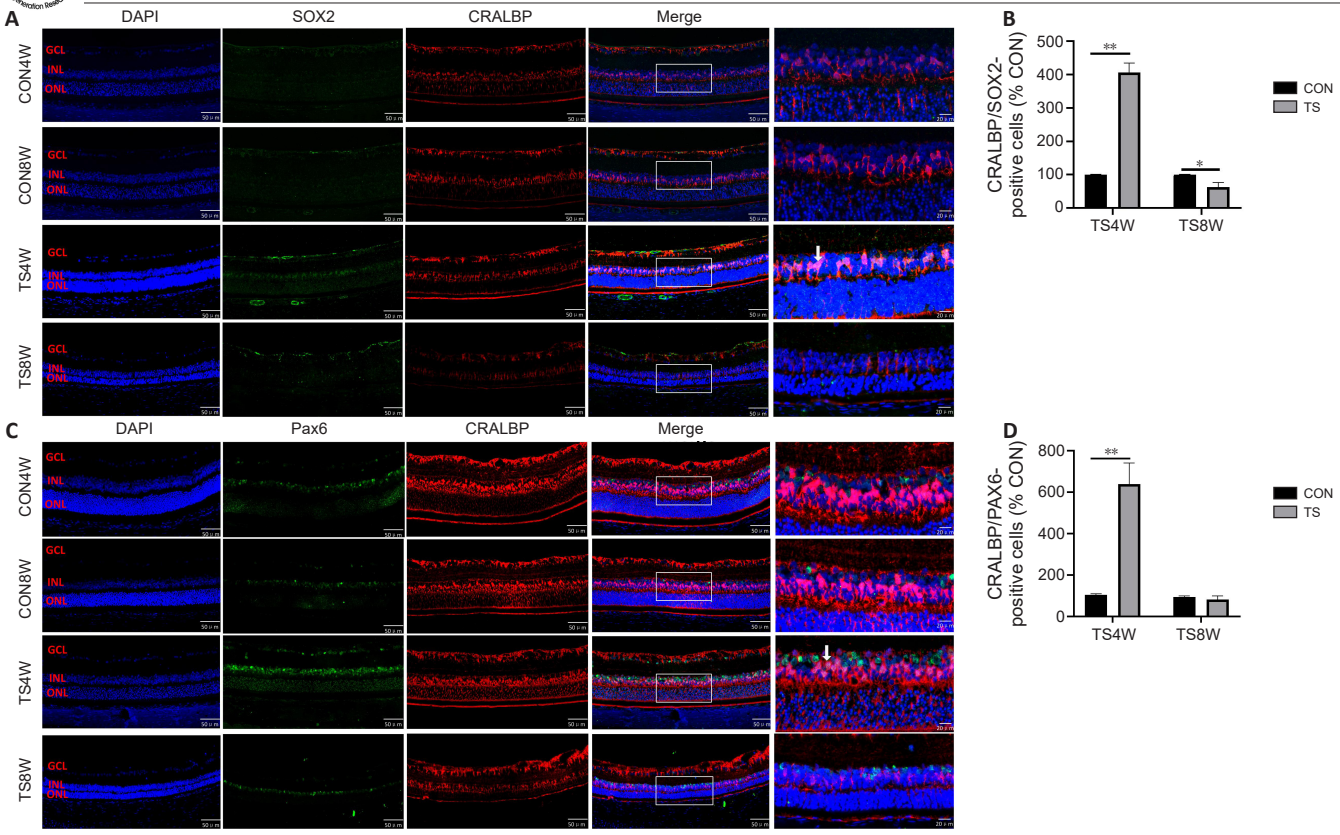

Figure 4 | **Effect of simulated weightlessness on Müller cell reverse differentiation.**
Immunofluorescence double staining of the rat retina. Red indicates the Müller cell marker CRALBP (Cy3), green indicates the progenitor cell marker SOX2 or PAX6 (Alexa Fluor™ 488), and blue indicates nuclear DAPI staining. (A) Representative images of CRALBP/SOX2 immunofluorescence. (B) CRALBP/SOX2-positive cells. There were more CRALBP/SOX2-positive cells in the TS4W group than in the CON4W group. (C) Representative immunofluorescence image of CRALBP/PAX6 staining. Scale bar: 20 μm (left four columns), 50 μm (rightmost column). (D) Quantification of CRALBP/PAX6-positive cells. There were more CRALBP/PAX6-positive cells in the TS4W group than in the CON4W group. Data are expressed as mean ± SD (n = 4 per group). *P < 0.05, **P < 0.01 (independent samples t-test). CON: Control; CRALBP: cellular retinaldehyde-binding protein; DAPI: 4′,6-diamidino-2-phenylindole; GCL: ganglion cell layer; INL: inner nuclear layer; ONL: outer nuclear layer; PAX6: paired box gene 6; TS4W: tail suspension for 4 weeks; TS8W: tail suspension for 8 weeks.

after 8 weeks of tail suspension. Furthermore, SOX2, PAX6, crx, and rhodopsin expression levels were barely detectable following 8 weeks of tail suspension. However, we observed overexpression of GFAP, a Müller cell marker that is only expressed at very low levels in the normal retina. Increased retinal GFAP expression was observed in pathological injury to Müller cells, leading to overactivation and proliferation of Müller cells located in the subretinal space. Finally, a glial scar was formed with outer segmental debris, which exacerbates apoptosis of photoreceptor cells (Jian et al., 2015, 2017). Thus, transient repair cannot prevent degeneration and glial scar formation. Under normal conditions, Müller cells are responsible for uptake of excessive GLU from the synaptic gap through the GLU transporter GLAST; once inside the cell, GLU is transformed into non-neurotoxic glutamine by GS, which is then released into the extracellular area for further conversion to GLU by neuronal cells and released into the synaptic gap, i.e., the GLU cycle (Bringmann et al., 2009; Zhu et al., 2022). Müller cell gliosis can result from increased GFAP expression, which affects GLU metabolism, leading to GLU toxicity and exacerbating retinal degeneration.

Müller cells possess stem cell characteristics and are capable of generating neurotrophic and protective substances such as glial cell neurotrophic factor (GDNF), bFGF, insulin-like growth factor 1, and pigment epithelium-derived factor, among others. The neurotrophic factors are responsible for activating certain signaling pathways that target glial reprogramming andproliferation. This activation occurs through autocrine as well as paracrine mechanisms. The neurogenic potential of Müller cells can be activated by target-specific signaling pathways that trigger the glial response and promote differentiation into neurons (Igarashi et al., 2000; Sarthy et al., 2005; Sato et al., 2008; Goel and Dhingra, 2021; Zwanzig et al., 2021). bFGF has pro-angiogenic, trauma repair, tissue regeneration, and neuroprotective effects, and was found to be highly expressed among the upregulated differential proteins associated with retinal neuronal injury repair (Campbell et al., 2021; Duan et al., 2024). Moreover, human Müller cells cultured *in vitro* can differentiate into photoreceptor cells in response to treatment with bFGF, which can also induce the differentiation of mammalian Müller cells into retinal nerve cells. With the development of optic neuroprotection theory in recent years, the application of bFGF in ophthalmology is increasing, and most reports have focused on protecting retinal pigment epithelial cells and photoreceptor cells (Singhal et al., 2012). In addition, we found that MAP-1 is a highly expressed upregulated DEP. MAP-1 localizes to the

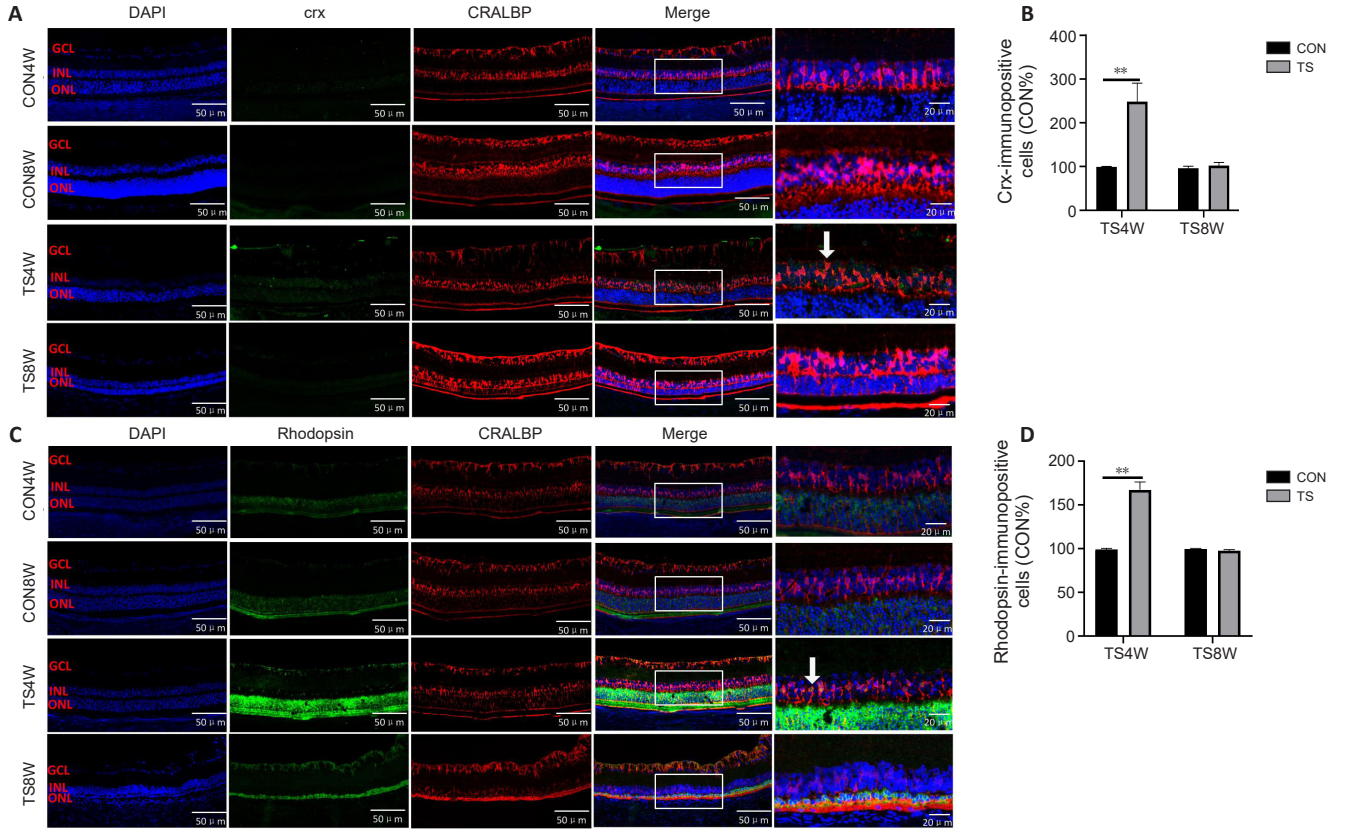

Figure 5 | **Effect of simulated weightlessness on Müller cell neural differentiation.**
Immunofluorescence double staining of the rat retina. Red indicates the retinal Muller cell marker CRALBP (Cy3), green indicates the retinal progenitor cell marker Crx or rhodopsin (Alexa Fluor™ 488), and blue indicates nuclear DAPI staining. (A) Immunofluorescence images of Crx staining. (B) Quantification of Crx-immunopositive cells. There were more Crx-immunopositive cells in the TS group than in the CON group. (C) Rhodopsin immunofluorescence images. Scale bar: 20 μm (left four columns), 50 μm (rightmost column). (D) Quantification of rhodopsin-immunopositive cells. There were more rhodopsin-immunopositive cells in the TS4W group than in the CON4W group. Data are expressed as mean ± SD (n = 4 per group). $^{**}P < 0.01$ (independent samples t-test). CON: Control; Crx: cone-rod homeobox; DAPI: 4′,6-diamidino-2-phenylindole; CRALBP: cellular retinaldehyde-binding protein; TS4W: tail suspension for 4 weeks; TS8W: tail suspension for 8 weeks.

surface of microtubules and has two variants: MAP-1A and MAP-1B. MAP-1B is crucial for neurite extension during embryonic development and contributes to the continued extension of the outer segments of adult photoreceptors. It is mainly distributed in the neuronal cytosol, perinuclear region, and extended axons; within the adult retina, it is mainly concentrated within the photoreceptor cell inner segments and cell bodies, with a relatively low distribution in the outer segments (Schoenfeld et al., 1989; Kinkl et al., 2001; Kang et al., 2014). As an intracellular factor, MAP-1B plays an essential regulatory role by protecting neuronal plasticity and migration, regulating the direction of axonal growth cone growth, promoting axonal extension and remyelination during nerve growth and regeneration, and participating in the repair of retinal neuronal damage (Hanley et al., 1999). Furthermore, we found that the neurotrophic factor GDNF was also highly expressed under conditions of simulated weightlessness, and was mainly distributed in the retina. In retinal lesions, Müller cells counteract neurons by expressing different levels of GDNF, and this GDNF-mediated neuroprotection indirectly protects photoreceptor cells. Currently, GDNF represents a novel therapeutic target for managing glaucoma and retinal ischemic lesions (Kucharska et al., 2014; Fu et al., 2015).

Our KEGG enrichment analysis demonstrated that the identified DEPs primarily participated in phototransduction, which is the process of converting light signals into electrical neural signals and occurs in the outer sections of photoreceptor cells. Research has demonstrated that mammalian Müller cells function as dynamic optical conduits, effectively directing light propagation within retinal tissue towards the photoreceptor cells. After 8 weeks of tail suspension (simulated weightlessness), the Müller cells had begun to glialize, which affected phototransduction by altering visually evoked potentials, delaying peak timing, and decreasing peak amplitude, reflecting impairment of the visual pathway.

Our findings suggest that Müller cells play a role in mediating degeneration of the outer nuclear layer of the retina in a simulated weightless environment. However, we did not perform an in-depth mechanistic exploration of the KEGG enrichment analysis results, which indicated that the DEPs mainly contributed to the PI3K-AKT signaling pathway. The PI3K-AKT signaling pathway can be activated by various stimuli and governs a range of crucial cellular mechanisms regulating cell progression and viability. Activated AKT modulates numerous cellular mechanisms, including cellular autophagy, cell cycle progression, and cell survival. The PI3K-AKT signaling pathway is potentially responsible for altering

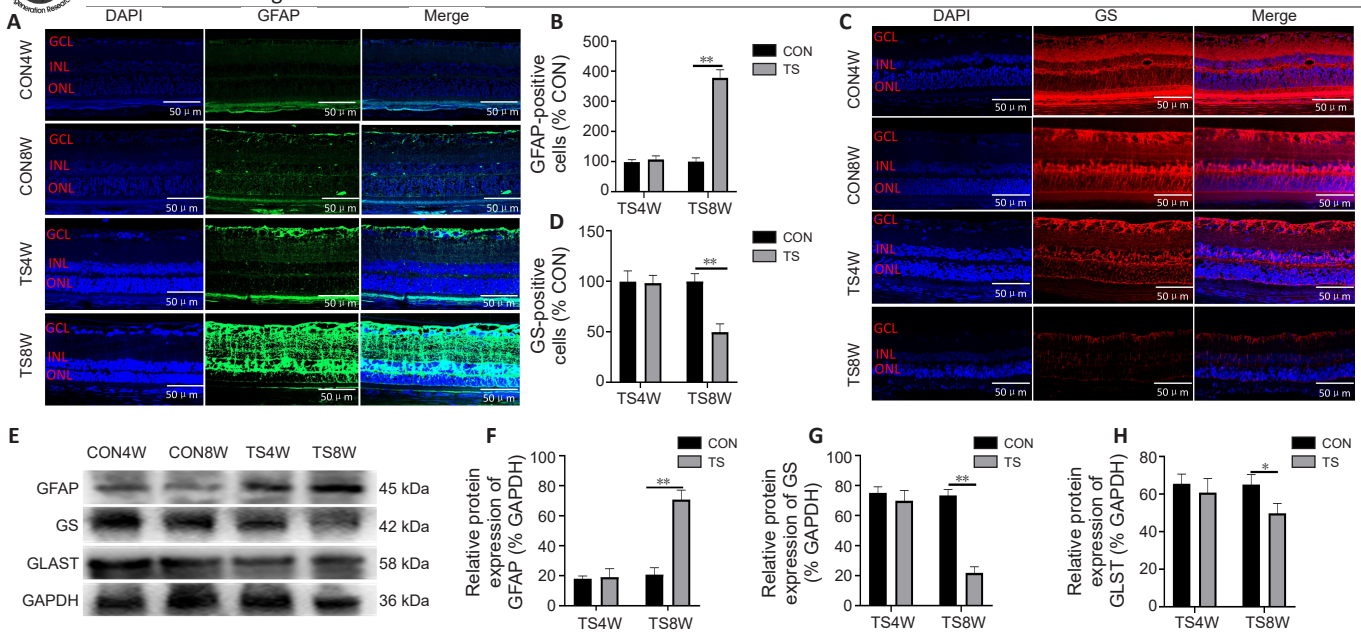

Figure 6 | **Simulated weightlessness can lead to Müller cell gelatinization.**
(A) Representative images of GFAP immunofluorescence (green, stained with Alexa Fluor™ 488). (B) Quantification of GFAP-immunopositive cells. There were more GFAP-immunopositive cells in the TS group than in the CON group. (C) Representative immunofluorescence images of GS (red, stained with Cy3). Scale bar: 50 μm. (D) Quantification of GS-immunopositive cells. There were more GS-immunopositive cells in the CON group than in the TS group. (E) Western blot of GFAP, GS, and GLAST. (F–H) Quantification of GFAP, GS, and GLAST relative protein expression. Data are expressed as mean ± SD (n = 4 per group). *P < 0.05, **P < 0.01 (independent samples t-test). CON: Control; DAPI: 4′,6-diamidino-2-phenylindole; GAPDH: glyceraldehyde-3-photosphate dehydrogenase; GCL: ganglion cell layer; GFAP: glial fibrous acidic protein; GLAST: L-glutamate/L-aspartate transporter; GS: glutamine synthetase; INL: inner nuclear layer; ONL: outer nuclear layer; TS: tail suspension.

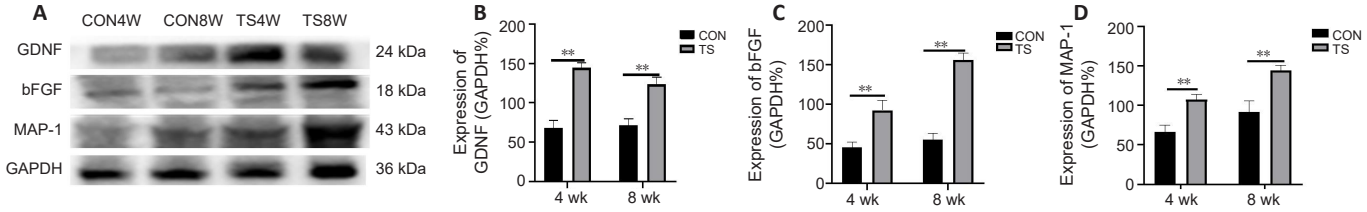

Figure 7 | **GDNF, bFGF, and MAP-1 expression in the retina of rats subjected to simulated weightlessness.**
(A) Representative western blot of GDNF, bFGF, and MAP-1. (B) Quantification of GDNF relative protein expression. GDNF expression in the TS group was higher than that in the CON group. (C) Quantification of bFGF relative protein expression. bFGF expression in the TS group was higher than that in the CON group. (D) Quantification of MAP-1 relative protein expression. MAP-1 expression in the TS group was higher than that in the CON group. Data are expressed as mean ± SD (n = 4 per group). **P < 0.01 (independent samples t-test). bFGF: Basic fibroblast growth factor; CON: control; GAPDH: glyceraldehyde-3-photosphate dehydrogenase; GDNF: glial cell-derived neurotrophic factor; MAP-1: microtubule-associated protein 1; TS: tail suspension.

protein expression in cases of retinal injury. Hence, future investigations will address the role of this signaling pathway in retinal injury.

In conclusion, weightlessness simulated by tail suspension can lead to degenerative changes in the outer nuclear layer of the retina and a decline in visual function, and Müller cells play a key role in this process. There were some limitations to the current study. On the International Space Station or during space flight, environmental impacts are more complex than simulated microgravity on earth, and include factors such as radiation, changes in circadian rhythms, increases in CO_2, changes in magnetic fields, vibrations, and other parameters. In this study, we used a classic tail suspension animal model to simulate a microgravity environment, and although a portion of the animal's body was suspended, its forelimbs remained in contact with the floor. However, under true microgravity conditions, due to zero gravity, the entire body floats weightlessly. Therefore, the results obtained in our terrestrial rodent model cannot be fully or accurately translated to the retinal diseases experienced by astronauts.

Acknowledgments: *The authors thank the Laboratory Animal Center of the Fourth Military Medical University for maintaining the rats used in this study.*

Author contributions: *ZZ and TC designed the conceptual framework of the study. YM and JX designed the experiments and wrote the manuscript. YM, DW, LY, XX, and YL performed the experiments. NZ and GY analyzed the data. All authors have read and approved the final version of the manuscript.*

Conflicts of interest: *None declared.*

Data availability statement: *The original contributions presented in the study are included in the article material, and further inquiries can be directed to the corresponding authors.*

Open peer reviewer: *Matteo Lulli, University of Florence, Italy.*

Additional files:

Additional Figure 1: *Repeatability analysis of different biological replicates used for iTRAQ-coupled LC-MS/MS proteomic analysis.*

Additional Table 1: *List of proteins differentially expressed by more than 1.3 times and lower than 1.3 times that of retina protein in rats suspended by tail for 8 weeks.*

Additional file 1: *Open peer review report 1.*

References

Association for Research in Vision and Ophthalmology (2021) ARVO Statement for the Use of Animals in Ophthalmic and Vision Research.

Bejarano-Escobar R, Sánchez-Calderón H, Otero-Arenas J, Martín-Partido G, Francisco-Morcillo J (2017) Müller glia and phagocytosis of cell debris in retinal tissue. J Anat 231:471-483.

Blottner D, Moriggi M, Trautmann G, Hastermann M, Capitanio D, Torretta E, Block K, Rittweger J, Limper U, Gelfi C, Salanova M (2023) Space omics and tissue response in astronaut skeletal muscle after short and long duration missions. Int J Mol Sci 24:4095.

Bringmann A, Pannicke T, Biedermann B, Francke M, Iandiev I, Grosche J, Wiedemann P, Albrecht J, Reichenbach A (2009) Role of retinal glial cells in neurotransmitter uptake and metabolism. Neurochem Int 54:143-160.

Campbell WA, Fritsch-Kelleher A, Palazzo I, Hoang T, Blackshaw S, Fischer AJ (2021) Midkine is neuroprotective and influences glial reactivity and the formation of Müller glia-derived progenitor cells in chick and mouse retinas. Glia 69:1515-1539.

Coughlin BA, Feenstra DJ, Mohr S (2017) Müller cells and diabetic retinopathy. Vision Res 139:93-100.

Dai X, Ye S, Chen X, Jiang T, Huang H, Li W, Yu H, Bao J, Chen H (2020) Rodent retinal microcirculation and visual electrophysiology following simulated microgravity. Exp Eye Res 194:108023.

Dou Y, Fei X, He X, Huan Y, Wei J, Wu X, Lyu W, Fei Z, Li X, Fei F (2024) Homer1a reduces inflammatory response after retinal ischemia/reperfusion injury. Neural Regen Res 19:1608-1617.

Duan H, Li S, Hao P, Hao F, Zhao W, Gao Y, Qiao H, Gu Y, Lv Y, Bao X, Chiu K, So KF, Yang Z, Li X (2024) Activation of endogenous neurogenesis and angiogenesis by basic fibroblast growth factor-chitosan gel in an adult rat model of ischemic stroke. Neural Regen Res 19:409-415.

Ercan E (2021) Effects of aerospace environments on the cardiovascular system. Anatol J Cardiol 25:3-6.

Fitzgerald W, Chen S, Walz C, Zimmerberg J, Margolis L, Grivel JC (2009) Immune suppression of human lymphoid tissues and cells in rotating suspension culture and onboard the International Space Station. In Vitro Cell Dev Biol Anim 45:622-632.

Fu S, Dong S, Zhu M, Sherry DM, Wang C, You Z, Haigh JJ, Le YZ (2015) Müller glia are a major cellular source of survival signals for retinal neurons in diabetes. Diabetes 64:3554-3563.

Galdamez LA, Brunstetter TJ, Lee AG, Tarver WJ (2020) Origins of cerebral edema: implications for spaceflight-associated neuro-ocular syndrome. J Neuroophthalmol 40:84-91.

Goel M, Dhingra NK (2021) bFGF and insulin lead to migration of Müller glia to photoreceptor layer in rd1 mouse retina. Neurosci Lett 755:135936.

Hanley JG, Koulen P, Bedford F, Gordon-Weeks PR, Moss SJ (1999) The protein MAP-1B links GABA(C) receptors to the cytoskeleton at retinal synapses. Nature 397:66-69.

He M, Long P, Chen T, Li K, Wei D, Zhang Y, Wang W, Hu Y, Ding Y, Wen A (2021) ALDH2/SIRT1 contributes to type 1 and type 2 diabetes-induced retinopathy through depressing oxidative stress. Oxid Med Cell Longev 2021:1641717.

Igarashi Y, Chiba H, Utsumi H, Miyajima H, Ishizaki T, Gotoh T, Kuwahara K, Tobioka H, Satoh M, Mori M, Sawada N (2000) Expression of receptors for glial cell line-derived neurotrophic factor (GDNF) and neurturin in the inner blood-retinal barrier of rats. Cell Struct Funct 25:237-241.

Ikeda C, Abe T, Sakai A, Hirasaka K, Nikawa T (2012) Space flight/bedrest immobilization and bone. Space flight and bed rest-mediated muscle atrophy. Clin Calcium 22:1813-1820.

Jha KA, Nag TC, Wadhwa S, Roy TS (2017) Immunohistochemical localization of GFAP and glutamate regulatory proteins in chick retina and their levels of expressions in altered photoperiods. Cell Mol Neurobiol 37:1029-1042.

Jian Q, Tao Z, Li Y, Yin ZQ (2015) Acute retinal injury and the relationship between nerve growth factor, Notch1 transcription and short-lived dedifferentiation transient changes of mammalian Müller cells. Vision Res 110:107-117.

Jurkute N, Robson AG (2021) Electrophysiology in neuro-ophthalmology. Handb Clin Neurol 178:79-96.

Kalesnykas G, Tuulos T, Uusitalo H, Jolkkonen J (2008) Neurodegeneration and cellular stress in the retina and optic nerve in rat cerebral ischemia and hypoperfusion models. Neuroscience 155:937-947.

Kang MH, Law-Davis S, Balaratnasingam C, Yu DY (2014) Sectoral variations in the distribution of axonal cytoskeleton proteins in the human optic nerve head. Exp Eye Res 128:141-150.

Karlen SJ, Miller EB, Burns ME (2020) Microglia activation and inflammation during the death of mammalian photoreceptors. Annu Rev Vis Sci 6:149-169.

Kergoat H, Durand MJ (1996) Correlating increased ocular and systemic blood pressures with neuroretinal function. Aviat Space Environ Med 67:1174-1178.

Kinkl N, Sahel J, Hicks D (2001) Alternate FGF2-ERK1/2 signaling pathways in retinal photoreceptor and glial cells in vitro. J Biol Chem 276:43871-43878.

Kondo M, Fujinami K, Horiguchi M, Local Organizers of ISCEV in Kyoto 2023 (2023) 60th annual symposium of the international society for clinical electrophysiology of vision (ISCEV 2023 Kyoto). Doc Ophthalmol 146:1-2.

Kucharska J, Del Río P, Arango-Gonzalez B, Gorza M, Feuchtinger A, Hauck SM, Ueffing M (2014) Cyr61 activates retinal cells and prolongs photoreceptor survival in rd1 mouse model of retinitis pigmentosa. J Neurochem 130:227-240.

Lee AG, Mader TH, Gibson CR, Tarver W, Rabiei P, Riascos RF, Galdamez LA, Brunstetter T (2020) Spaceflight associated neuro-ocular syndrome (SANS) and the neuro-ophthalmologic effects of microgravity: a review and an update. NPJ Microgravity 6:7.

Leinonen HO, Bull E, Fu Z (2023) Neural and Müller glial adaptation of the retina to photoreceptor degeneration. Neural Regen Res 18:701-707.

Lin YP, Ouchi Y, Satoh S, Watanabe S (2009) Sox2 plays a role in the induction of amacrine and Müller glial cells in mouse retinal progenitor cells. Invest Ophthalmol Vis Sci 50:68-74.

Morey-Holton ER, Globus RK (1998) Hindlimb unloading of growing rats: a model for predicting skeletal changes during space flight. Bone 22:83s-88s.

Morey-Holton ER, Globus RK (2002) Hindlimb unloading rodent model: technical aspects. J Appl Physiol (1985) 92:1367-1377.

Navasiolava N, Yuan M, Murphy R, Robin A, Coupé M, Wang L, Alameddine A, Gauquelin-Koch G, Gharib C, Li Y, Custaud MA (2020) Vascular and microvascular dysfunction induced by microgravity and its analogs in humans: mechanisms and countermeasures. Front Physiol 11:952.

Niu L, Fang Y, Yao X, Zhang Y, Wu J, Chen DF, Sun X (2021) TNFα activates MAPK and Jak-Stat pathways to promote mouse Müller cell proliferation. Exp Eye Res 202:108353.

Ong J, Tavakkoli A, Strangman G, Zaman N, Kamran SA, Zhang Q, Ivkovic V, Lee AG (2022) Neuro-ophthalmic imaging and visual assessment technology for spaceflight associated neuro-ocular syndrome (SANS). Surv Ophthalmol 67:1443-1466.

Qu J, Zhao H, Li Q, Pan P, Ma K, Liu X, Feng H, Chen Y (2018) MST1 suppression reduces early brain injury by inhibiting the NF-κB/MMP-9 pathway after subarachnoid hemorrhage in mice. Behav Neurol 2018:6470957.

Reichenbach A, Bringmann A (2020) Glia of the human retina. Glia 68:768-796.

Reichenbach A, Wurm A, Pannicke T, Iandiev I, Wiedemann P, Bringmann A (2007) Müller cells as players in retinal degeneration and edema. Graefes Arch Clin Exp Ophthalmol 245:627-636.

Sarthy VP, Pignataro L, Pannicke T, Weick M, Reichenbach A, Harada T, Tanaka K, Marc R (2005) Glutamate transport by retinal Muller cells in glutamate/aspartate transporter-knockout mice. Glia 49:184-196.

Sato T, Fujikado T, Morimoto T, Matsushita K, Harada T, Tano Y (2008) Effect of electrical stimulation on IGF-1 transcription by L-type calcium channels in cultured retinal Müller cells. Jpn J Ophthalmol 52:217-223.

Schoenfeld TA, McKerracher L, Obar R, Vallee RB (1989) MAP 1A and MAP 1B are structurally related microtubule associated proteins with distinct developmental patterns in the CNS. J Neurosci 9:1712-1730.

Singhal S, Bhatia B, Jayaram H, Becker S, Jones MF, Cottrill PB, Khaw PT, Salt TE, Limb GA (2012) Human Müller glia with stem cell characteristics differentiate into retinal ganglion cell (RGC) precursors in vitro and partially restore RGC function in vivo following transplantation. Stem Cells Transl Med 1:188-199.

Song K, Lin Z, Cao L, Lu B, Chen Y, Zhang S, Lu J, Xu H (2023) Sox11b regulates the migration and fate determination of Müller glia-derived progenitors during retina regeneration in zebrafish. Neural Regen Res 18:445-450.

Szabó-Salfay O, Pálhalmi J, Szatmári E, Barabás P, Szilágyi N, Juhász G (2001) The electroretinogram and visual evoked potential of freely moving rats. Brain Res Bull 56:7-14.

Taibbi G, Cromwell RL, Kapoor KG, Godley BF, Vizzeri G (2013) The effect of microgravity on ocular structures and visual function: a review. Surv Ophthalmol 58:155-163.

Visual Physiology Group of Ophthalmology Branch of Chinese Medical Association, Visual Physiology Group of Chinese Ophthalmologist Association (2023) Chinese expert consensus on the clinical visual electrophysiologic examination terminology (2023). Chin J Ophthalmol 59:174-180.

Wachtmeister L (1998) Oscillatory potentials in the retina: what do they reveal. Prog Retin Eye Res 17:485-521.

Wang D, Zhao M, Tang X, Gao M, Liu W, Xiang M, Ruan J, Chen J, Long B, Li J (2023) Transcriptomic analysis of spinal cord regeneration after injury in Cynops orientalis. Neural Regen Res 18:2743-2750.

Wojcik P, Kini A, Al Othman B, Galdamez LA, Lee AG (2020) Spaceflight associated neuro-ocular syndrome. Curr Opin Neurol 33:62-67.

Wunderlich KA, Leveillard T, Penkowa M, Zrenner E, Perez MT (2010) Altered expression of metallothionein-I and-II and their receptor megalin in inherited photoreceptor degeneration. Invest Ophthalmol Vis Sci 51:4809-4820.

Xiong Y, Ji H, You Z, Yao F, Zhou R, Song W, Xia X (2019) Otx2 enhances transdifferentiation of Müller cells-derived retinal stem cells into photoreceptor-like cells. J Cell Mol Med 23:943-953.

Xu D, Zhong LT, Cheng HY, Wang ZQ, Chen XM, Feng AY, Chen WY, Chen G, Xu Y (2023) Overexpressing NeuroD1 reprograms Müller cells into various types of retinal neurons. Neural Regen Res 18:1124-1131.

Yang JQ, Jiang N, Li ZP, Guo S, Chen ZY, Li BB, Chai SB, Lu SY, Yan HF, Sun PM, Zhang T, Sun HW, Yang JW, Zhou JL, Yang HM, Cui Y (2020) The effects of microgravity on the digestive system and the new insights it brings to the life sciences. Life Sci Space Res (Amst) 27:74-82.

Yang JW, Song QY, Zhang MX, Ai JL, Wang F, Kan GH, Wu B, Zhu SQ (2022) Spaceflight-associated neuro-ocular syndrome: a review of potential pathogenesis and intervention. Int J Ophthalmol 15:336-341.

Zhang LF, Hargens AR (2018) Spaceflight-induced intracranial hypertension and visual impairment: pathophysiology and countermeasures. Physiol Rev 98:59-87.

Zhao HW, Zhao J, Hu LN, Liang JN, Shi YY, Nie C, Qiu CY, Nan XS, Li YX, Gao FL, Liu Y, Dong Y, Luo L (2016) Effect of long-term weightlessness on retina and optic nerve in tail-suspension rats. Int J Ophthalmol 9:825-830.

Zhu M, Gao S, Gao S, Wang Y, Li N, Shen X (2022) Interleukin-17A attenuates photoreceptor cell apoptosis in streptozotocin-induced diabetic mouse model. Bioengineered 13:14175-14187.

Zwanzig A, Meng J, Müller H, Bürger S, Schmidt M, Pankonin M, Wiedemann P, Unterlauft JD, Eichler W (2021) Neuroprotective effects of glial mediators in interactions between retinal neurons and Müller cells. Exp Eye Res 209:108689.

C-Editor: Zhao M; S-Editors:Yu J, Li CH; L-Editors: Crow E, Song LP; T-Editor: Jia Y